Construction and Building Materials 220 (2019) 76–89

Contents lists available at ScienceDirect

Construction and Building Materials

journal homepage: www.elsevier.com/locate/conbuildmat

Silica aerogel/polyester blankets for efficient sound absorption in buildings

Zahra Talebi, Parham Soltani *, Negar Habibi, Fatemeh Latifi

Department of Textile Engineering, Isfahan University of Technology, Isfahan 84156-83111, Iran

HIGHLIGHTS

- Lightweight sound absorbers with long service life were produced.
- Silica aerogel/PET blankets enjoy higher SAC than their untreated counterparts.
- SAC is strongly affected by the pore structure and density of aerogel particles.
- Hydrophobic aerogels/PET blanket for sound absorption applications were produced.
- Hydrophobic aerogel blankets show higher SAC as compared with hydrophilic blankets.

GRAPHICAL ABSTRACT

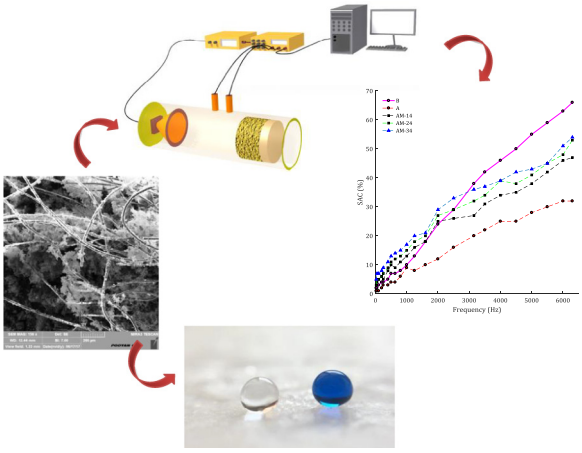

ARTICLE INFO

Article history:
Received 23 November 2018
Received in revised form 8 May 2019
Accepted 3 June 2019
Available online 6 June 2019

Keywords:
Acoustic characteristics
Silica aerogel blanket
Polyester nonwoven
Pore structure
Hydrophobicity
X-ray micro-computed tomography

ABSTRACT

In this paper sound absorption characteristics of silica aerogel/polyester (PET) blankets are investigated. PET fibers were made on an industrial scale compact melt spinning line and then processed on a laboratory scale needling line to produce nonwoven fabrics. The silica aerogel blankets were prepared by *in situ* synthesis of silica aerogel on the nonwoven fabrics via a two-step sol-gel process of tetraethoxysilane which was followed by drying at ambient pressure. In order to achieve aerogel particles with different pore structure and properties, various synthesis conditions were used. The nonwoven samples were characterized in terms of thickness, fiber diameter, porosity and pore size by X-ray micro-computed tomography and scanning electron microscopy. Moreover, nitrogen adsorption analysis was carried out to determine the specific surface area and pore structure of aerogel particles.

The effect of pore structure, physical properties and hydrophobicity of aerogel particles on sound absorption coefficient (SAC) of blankets was investigated using two-microphone transfer function method. Also, the effect of sol volume and nonwoven thickness was investigated. The results indicated that at all frequency levels, silica aerogel/PET blankets enjoy higher SAC than their untreated counterparts. It was found that, SAC is strongly affected by the pore structure of aerogel particles. Silica aerogels with lower bulk densities, larger pore size and higher porosities exhibited better sound absorption

* Corresponding author.
E-mail address: Pa.soltani@cc.iut.ac.ir (P. Soltani).

https://doi.org/10.1016/j.conbuildmat.2019.06.031

performance. The results also indicated that hydrophobic aerogel blankets exhibit higher SAC as compared with hydrophilic blankets. The results also showed that the thickness of nonwoven fabric strongly affects the SAC of aerogel blankets.

1. Introduction

In recent decade, noise pollution has become the most widespread and least controlled environmental issue. Noise pollution causes or contributes to not only psychological disorders, but also cardiovascular disease, loss of hearing, high blood pressure and tinnitus hearing impairment. Thus technological control of acoustical behavior of industrial products is a fact that has to be scientifically faced by researchers [1]. This control can be achieved using either sound insulating or sound absorbing materials. Conventional various sound absorbers such as foam-like materials or nonwoven fabrics as low-density porous materials can prevent reflection of the incident sound waves and hence increase sound absorption. The use of nonwovens, as widely accepted porous sound absorbing materials, has been extensively researched [2–6].

Since more than a decade, acoustic engineers have been looking for lightweight sound absorbing materials in buildings. The challenge primarily stemmed from inability of conventional bulky nonwoven fabrics and foams to absorb sound waves, specifically sound waves of low frequency bands that impair speech comprehension [7,8]. According to the Mass Law, for low-frequency sound waves, by doubling the mass per unit area of a single layer of nonwoven fabric, the mean sound transmission loss by the fabric increases at an approximate constant rate of 6 dB due to the increase in inertia forces [9]. Thus the current lightweight materials such as nonwovens and acoustical foams cannot fully meet the technical criteria that are required by acoustic engineers. These demands may be thought of be fulfilled by scientifically designed multilayered structures, which are not always a practical engineering solution due to either thick panels or heavy structures [10,11].

In contrast to conventional acoustic materials, silica aerogels are quasi-stable low-density assemblies of nano-particles. These materials were initially used as highly effective thermal insulations or as nano-porous hosts of functional guests. These promising nanomaterials are commonly synthesized by the sol–gel process followed by a supercritical drying technique. Silica aerogel as a mesoporous material is composed of internally cross-linked structure of SiO_2 chains with large number of pores which are filled with air. Silica aerogels benefit from a high specific surface area as 300–1000 m^2/g, porosity as high as 98% air and 2% open pores, density as low as 0.05–0.5 g/cm^3, and thermal conductivity of 0.014 W/mK which is remarkably lower than any other commercially available insulating materials [12,13]. Such diverse characteristics that are unique to aerogels have yielded the use of these materials in a wide range of commercial and high-tech end-uses that comprise buildings, automotive, acoustics, optics, electronics and clothing.

2. Background

While the optical and thermal characteristics of silica aerogels for building insulation is extensively reported in the literature [14–19], the attempts for precise determination of their acoustic behavior are still scarce [20–23]. In aerogels, amplitude and velocity attenuation of an acoustic wave occurs due to progressive transfer of wave energy from the gas to aerogel solid network. This results in sound velocity of about 100 m/s which is 1/3 of the velocity of sound in air. Low velocity of sound in silica aerogels as well as acoustic impedance that is tunable with production conditions make them more suitable for acoustic applications [24].

The acoustic properties of silica aerogels are greatly influenced by various parameters such as interstitial gas type and Young's modulus of the silica aerogel skeleton structure [25]; different chemical reactions during gelation stage of aerogel formation [26]; aerogel density and texture [27], and the change in the ratio of characteristics impedance between the medium and the absorption material [28]. Riffat and Qiu [29] have stated that in addition to these factors, the type of reinforcement can also strongly affect the acoustic behavior of silica aerogels.

Sachithanadam and Joshi [20] investigated the effect of silica aerogel granules of various sizes from 0.5 to 3.35 mm on acoustic properties of protein-based silica aerogels and found that sound absorption coefficient (SAC) is inversely proportional to granule size. Buratti et al. [21] investigated the effect of granules size on acoustic behavior of granular aerogels and found that the smallest granules exhibit highest density and enjoy highest acoustic insulation. Bheekhun et al. [22] pointed to suitability of silica aerogels as highly valued airborne ultrasonic transducers due to their low modulus which is adjustable during synthesis stage. Cotana et al. [23] performed in-field investigation of thermal energy, acoustic and lighting performance of innovative glazing systems filled with aerogel granules. It was found that high correlation exists among these three properties. The results showed the aerogel capability to increase the facade acoustic insulation index by 3 dB.

Despite advantageous properties, due to high manufacturing cost and hazardous supercritical drying operation, the use of silica aerogels as sound absorber materials has been hindered. Thus, acoustic application of the silica aerogels has been rather limited to space exploration [30]. More recently, the hazardous supercritical drying operation in silica aerogel synthesis has been replaced by drying at the atmospheric pressure [31,32]. The inherent structural fragility of silica aerogels is an additional stumbling block that has prevented their full commercialization. The fragility of silica aerogels can be overcome by incorporation of polymers and fibers in the silica network. Recently reinforced flexible nonwoven blankets embedded by aerogels particles in which the brittle silica aerogel network is supported by the fibrous matrix have been developed [33–35]. This pioneering and beneficial development has opened the path to many other end-uses for silica aerogels.

Motahari et al. [33] investigated the sound absorption behavior of silica aerogel blankets prepared by cotton nonwovens as the fibrous matrix and studied the effect of aging time on SAC. The results showed that SAC is influenced by the density and structural properties of silica aerogel which can be affected by the processing conditions. It was found that silica aerogel considerably increased the sound absorption of cotton nonwovens up to 2500 Hz. However, at high frequency bands aerogel treated cotton nonwovens irrespective of their aerogel densities suffer from lower SAC as compared with untreated cotton nonwoven. Eskandari et al. [34] investigated the acoustic behavior of silica aerogel/UPVC blankets and stated that SAC of UPVC increases up to three times due to addition of silica aerogel into the UPVC matrix. Yang et al. [35] investigated acoustic behavior of polyethylene/polyester nonwoven fabrics embedded with silica aerogel. In contrast with previous published works, decrease in SAC with increasing aerogel content was reported.

The above review is by no means exhaustive; however it highlights the promising effect of silica aerogel on acoustic behavior of fibrous media. The reported results on the effect of embedding aerogel on acoustic behavior of fibrous porous networks appeared to be contradictory. Moreover, most of the investigations on the acoustic characteristics of aerogels deal with monolithic aerogels [36–38], whereas researches on acoustic properties of granular aerogels are very scarce. Additionally, due to the destructive hydrophilic nature of the aerogel the structural integrity of the aerogel cannot be sustained over long period of time, which results in short service life of the aerogel embedded blankets. Previous works on the aerogels have failed to address the effect of synthesis conditions and hydrophilicity of aerogels on SAC. Thus this work aims to evaluate the sound absorption behavior of silica aerogel/PET blankets with view to the effect of aerogel pore structure and physical properties. Moreover, the effect of processing parameters such as sol volume used in the immersion step of aerogel blanket synthesis and nonwoven fabric thickness is also investigated. Additionally in order to overcome both the limitation of the previous works and prolong the service life of the aerogel embedded blanket for noise control applications, hydrophobic properties of blankets are also evaluated.

3. Experimental

3.1. Materials

TEOS (tetraethoxysilane), TMCS (tetramethylchlorosilane), ethanol, hydrochloric acid and ammonia were supplied from Merck (Darmstadt, Germany). N-hexane was purchased from Dr. Mojallali Industrial Chemical Complex (Arak, Iran). TG641 polyester granules (textile grade) produced by Arak Petrochemical Company (Arak, Iran) were used to make the nonwoven test samples.

3.2. Needled nonwovens production

In this study polyester (PET) needle punched nonwoven fabrics which have gained expanding use in industrial acoustic applications are used as the reinforcement substrates. Needle punching technology accounts for 20–25% of global total nonwoven production. In this process due to the action of a series of barbed needles, fibers of a carded web are consolidated. The consolidation of the fibrous web depends on numerous factors such as frequency of the reciprocating needle board, type of needles, needle penetration distance, linear speed of the fibrous web, density of the needle in the needle board and characteristics of the fibrous web [39].

In this study two needled nonwoven fabrics coded by A and B were investigated. Sample A was provided by Bibaft Co., (Tehran, Iran). In order to produce sample B, melt-spun PET fibers with fineness of 5 dtex and density of 1.38 g/cm^3 were produced on a six positions one-stage industrial scale compact melt spinning line in Mahoot Co. (Isfahan, Iran). Fibers were then processed on a 50-centimeter-wide carding section of the laboratory scale needling line, which is equipped with randomizing rollers. The randomized webs were fed to the horizontal cross-lapper of the line to produce multilayer fibrous structure which is called batt. This crossed laid batt at the required weight and thickness was transferred to the needling section of the line. The fibrous batt was consolidated by the action of the needles and the needle felted fabric was eventually taken-up. The needling operation was adjusted such that the imparted punch density to sample was 160/cm^2 at needle penetration depth of 11 mm using Groz-Beckert felting needles 15 × 18 × 32 × 3 C333 G3007. Nonwoven samples were prepared at temperature of 20 ± 2 °C and relative humidity of 65 ± 2%. Fig. 1 shows the laboratory needle punching production line. Characteristics of the needled samples are shown in Table 1.

Fig. 1. Laboratory needle punching production line.

Table 1
Characteristics of nonwoven samples.

Sample code	Fabric thickness (μCT*) (mm)	Fabric thickness (Experimental) (mm)	Mass per unit area (g/m^2)	Fabric porosity (μCT) (%)	Fabric porosity (Experimental) (%)	Fiber diameter (μCT) (μm)
A	2.67	2.58	206	94.24	93.98	17.60
B	6.35	6.29	834	90.39	91.04	29.45

* μCT: Micro-computed tomography.

Table 2
The aerogel blankets synthesis conditions.

Sample code	TEOS:H_2O:EtOH:HCl:NH_3 Molar ratio	Gelation Temp. (°C)	Ageing		Surface modification Temp. (°C)
			Solvent	Temp. (°C)	
AC-24 BC-24	1:3.5:3.9:24 × 10^{-4}:14 × 10^{-3}	50	EtOH	12 h at 45 °C and 12 h at 30 °C	45
AI-24 BI-24	1:3.5:3.9:24 × 10^{-4}:14 × 10^{-3}	50	77.5% EtOH + 15% TEOS + 7.5% H_2O	12 h at 45 °C in ageing solvent and 12 h at 45 °C in EtOH	–
AM-14 AM-24 AM-34 BM-14 BM-24 BM-34	1:6:3.9:24 × 10^{-4}:28 × 10^{-3}	50	EtOH	12 h at 45 °C and 12 h at 30 °C	45
AH-24 BH-24	1:2.8:3.9:12 × 10^{-4}:7 × 10^{-3}	50	EtOH	12 h at 45 °C and 12 h at 30 °C	45

3.3. Aerogel blankets preparation

An aerogel blanket is a composite of a granular silica aerogel and nonwoven reinforcement that turns the brittle aerogel into a durable, flexible/solid material, useful for building envelopes, inside or outside. Fabrics samples of 12 cm × 12 cm were firstly washed to remove any spin-finish and possible impurities existing in the nonwoven fabrics by soaking the fabrics in ethanol for 1 h at 30 °C. Afterwards, samples rinsed for 60 min and air dried at 100 °C. The silica aerogel blankets were prepared by in situ synthesis of silica aerogel on the PET nonwoven fabrics via a two-step sol-gel process of TEOS which was followed by drying at ambient pressure. Upon preparation of silica sol during hydrolysis stage, nonwoven fabrics were soaked in the silica sol at 60 °C for 30 min. The specimens were then cooled to 30 °C and the gelation step was achieved with water and ammonia in pH of 7–8 followed by keeping at 50 °C for 1.5 h to strengthen the structure of the gel. After gelation, the aerogel blankets were aged in ethanol for 24 h and then the solvent exchange process was done in n-hexane for 24 h. The surface modification step for hydrophobic samples was carried out by 5% TMCS in the n-hexane for 12 h at 45 °C and then the samples were washed with n-hexane for 12 h. Finally, the drying process was performed in 12 h at room temperature, 5 h at 60 °C, 5 h at 80 °C, and 2 h at 120 °C. The surface modification step was omitted from synthesis process for preparation of hydrophilic blanket samples and the aging conditions were changed according to Table 2. For more information about the aerogel blankets preparation readers are referred to previous works of authors [40,41].

In order to investigate the effect of pore structure of silica aerogel on the sound absorption performance, various aerogel blankets were prepared at different synthesis conditions according to Table 2. In this table each silica aerogel blanket sample is coded with XY-Z. Where X can be A or B and denotes the type of aerogel-free neat samples, Y represents the aerogel particle type obtained in different synthesis conditions and Z shows the sol volume used in the immersion step of blankets.

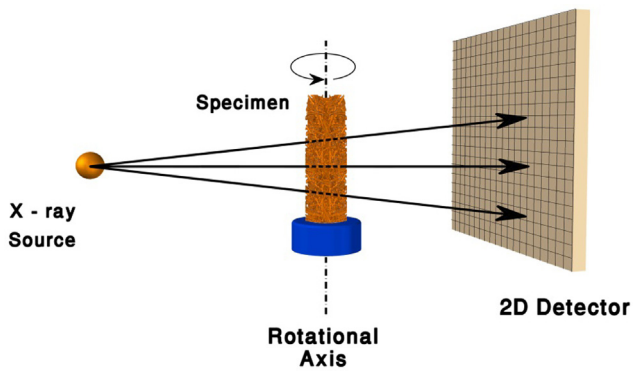

Fig. 2. Schematic of μCT system.

3.4. Image acquisition via X-ray micro-computed tomography

The internal microstructure of nonwovens was obtained using nondestructive X-ray micro-computed tomography (μCT) at the University of Huddersfield (Huddersfield, UK). The imaging was performed with the laboratory X-ray computed tomography device CT Pro (Nikon Metrology, Tring, UK) equipped with a metal-oxide semiconductor (CMOS) 1000 × 1000 pixel flat panel detector. The apparatus consists of three main components: an X-ray source, a series of digital detectors that measures X-ray intensity attenuation along multiple beam paths, and a rotating sample holder. Fig. 2 shows the schematic of μCT system.

Principally, X-ray attenuation measurements taken around the object from different directions produce cross-sectional images of an object. X-rays transmitted through the material are absorbed according to a linear attenuation coefficient that has some spatial variation depending on the atomic number, local density and thickness of the material. A series of detectors captures the transmitted X-ray radiation and provide the numerical data required for reconstruction of an image [42,43].

From each nonwoven fabric, three samples of 5 mm × 5 mm were carefully cut using a diamond blade. Precautions were taken to ensure that the initial micro-structure of the samples is not changed. Afterwards, the samples were fixed on the rotating holder between X-ray source and detectors and progressively rotated to obtain radiographic projections within the entire range of 0–360° at 0.5° intervals. In order to provide enough space to obtain a reasonable sample-area from which to calculate the porosity of the sample as well as to provide a high resolution to render the fibers a viewing area of 6 mm × 6 mm was chosen [44]. The images were acquired at 120 kV and 110 μA. All the scans were performed with the same spatial resolution of 3 μm per voxel. Computational volume reconstruction was performed with the Phoenix software datos|x by an ultra-high resolution noise-reducing filter back-projection algorithm with beam hardening and radiation fluctuation correction algorithms. Data rendered with Volume Graphics VGStudio MAX 2.2 (Volume Graphics Inc., Germany) was post-processed with MATLAB R2015a Image Processing Toolbox (The Mathworks Natick MA). The full details of post-processing image analysis including image de-noising and thresholding steps are given in the recent work of authors [45].

3.5. Measurement and characterizations

Prior to the tests, according to ASTM D1776M-16 "*Standard Practice for Conditioning and Testing Textiles*" samples were conditioned at relative humidity of 65 ± 2% and temperature of 20 ± 2 °C for 24 h and subsequently were characterized in terms of thickness, mass per unit area, porosity, fiber diameter, morphology, specific surface area, pore structure, hydrophobicity and sound absorption behavior.

3.5.1. Thickness

Thickness of the samples was experimentally measured using the original nonwovens according to ASTM D5729-97 "*Standard Test Method for Thickness of Nonwoven Fabrics*" at constant pressure level of 3.45 kPa at 10 different locations. Sample thickness was also measured using the 3D images obtained from μCT. Considering the possible compression of fabrics during experimental measurement and possible slight alternation of micro-structure during sample preparation for μCT imaging, a good agreement was observed between these two measurements. The results are presented in Table 1.

3.5.2. Mass per unit area

Mass per unit area of samples was determined according to ASTM D3776-07 "*Standard Test Method for Mass per Unit Area of Fabrics*". 10 samples of 10 cm × 10 cm were cut randomly from different locations of nonwoven samples and weighed by means of a precision digital balance (Shimadzu Corporation, Japan). The results are presented in Table 1.

3.5.3. Porosity

The porosity of samples was experimentally measured using the following equation:

$$\varepsilon = 1 - \frac{\rho_{fabric}}{\rho_{fiber}} \tag{1}$$

where ε is fabric porosity, and ρ_{fabric} and ρ_{fiber} respectively denote fabric and fiber density.

The porosity was also calculated from the 3D reconstructed image by simple calculation of the ratio of black voxels representing voids to the total number of voxels in the image. A good agreement was observed between these two measurements. The results are presented in Table 1.

3.5.4. Pore structure analysis

The surface morphology of the blankets and nonwoven fabrics samples was characterized by scanning electron microscopy (Tescan Mira, Czech) and μCT. Nonwovens pore size distribution was measured using image analysis of 3D μCT images. Full details of image analysis techniques are presented in recent work of authors [45] and research work of Mangan and Whitaker [46]. Briefly, in this method the identification is based on an Euclidean distance map, in which each pore voxel's distance to the nearest fiber phase is calculated. A watershed transformation is applied to this distance map to separate the pore space into pore objects. In order to identify distinct pores, seed regions of the watershed are introduced at the center of the pore objects and allowed to expand until they encounter another growing pore region.

For a given pore object, the equivalent diameter is equal to the diameter of the spherical pore of same volume. Therefore, the equivalent diameter is calculated using Eq. (2):

$$\text{Equivalent diameter} = \sqrt[3]{\frac{6 \times \textit{volume of pore object}}{\pi}} \tag{2}$$

Note that the μCT device used for this study has a resolution of 1–3 μm, which prevented the characterization of the aerogels. The nitrogen adsorption analysis (TriStar II plus, USA) and BET and BJH techniques were carried out on the silica aerogel particles to determine the specific surface area and pore structure of aerogels.

3.5.5. Hydrophobicity analysis

The hydrophobicity of aerogel blankets was evaluated from water contact angle of aerogel blankets measured by the sessile drop method.

3.5.6. Sound absorption measurement

The sound absorption coefficient (SAC) is defined as the ratio of the absorbed sound energy to the incident acoustic energy over

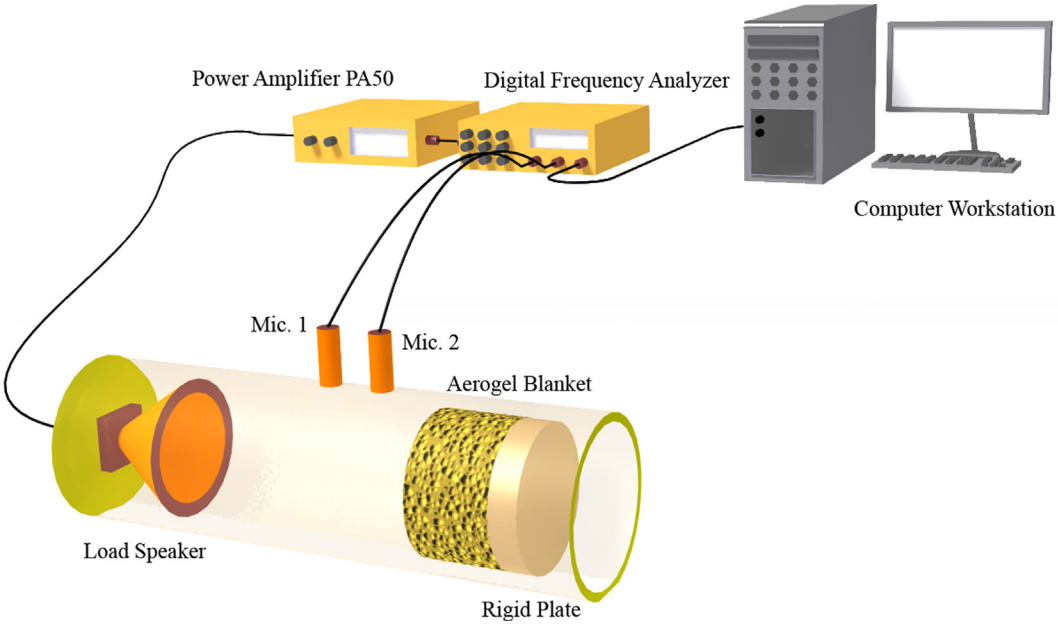

Fig. 3. Schematic of acoustic absorption apparatus.

specific frequency bands. This coefficient can be measured by various methods such as the reverberant field methods, steady-state methods and impedance tube methods, among which impedance tube is widely used to measure the SAC of acoustically soft materials. SACs of the test samples over the entire frequency range of 50–6100 Hz were measured using a BSWA double-microphones standing wave impedance tube (model SW420-470) which is schematically shown in Fig. 3. The tests were carried out under pressure and temperature conditions of 101 kPa and 20 °C according to ASTM E1050 (*Standard Test Method for Impedance and Absorption of Acoustical Materials Using a Tube, Two Microphones and a Digital Frequency Analysis System*).

Circular samples with diameters of 100 and 29 mm were used for SAC measurements at low frequency band of 50–1600 Hz and high frequency band of 1600–6100 Hz, respectively. The measuring system consists of a loudspeaker, a digital frequency analyzer unit (model MC 3242), two impedance tubes with diameters of 100 and 29 mm, a power amplifier (model PA50), two BSWA 1/4″ microphones (model MPA416) plus other necessary ancillaries. The loudspeaker which generates broadband plane sound waves of well-defined frequencies is mounted at the left end of the impedance tube and the test sample is fastened to the rigid right end of the tube as shown in Fig. 3.

A standing-wave interference pattern is generated due to the superposition of incident and reflected sound waves inside the tube. The SAC of the material can be determined by simultaneous measurement of sound pressure using two microphones positioned at two fixed locations. Finally a two-channel digital frequency analyzer measures the response of the two microphones and calculates SAC as a function of sound frequency. In order to minimize the experimental error, in this work average of three tests are reported. In order to present a single number index of the sound-absorbing efficiency of aerogel blankets, the SAC at frequencies of 250, 500, 1000 and 2000 Hz were averaged to obtain the noise reduction coefficient (NRC).

4. Results and discussion

4.1. Morphology of the samples

Visualization of the reconstructed geometry for neat (untreated) nonwoven fabrics A and B are shown in Fig. 4. As is observed both samples enjoy high complex structure which is a prerequisite for sound absorbing applications. Fig. 5 shows separated pores which are displayed using a cyclic colormap so that

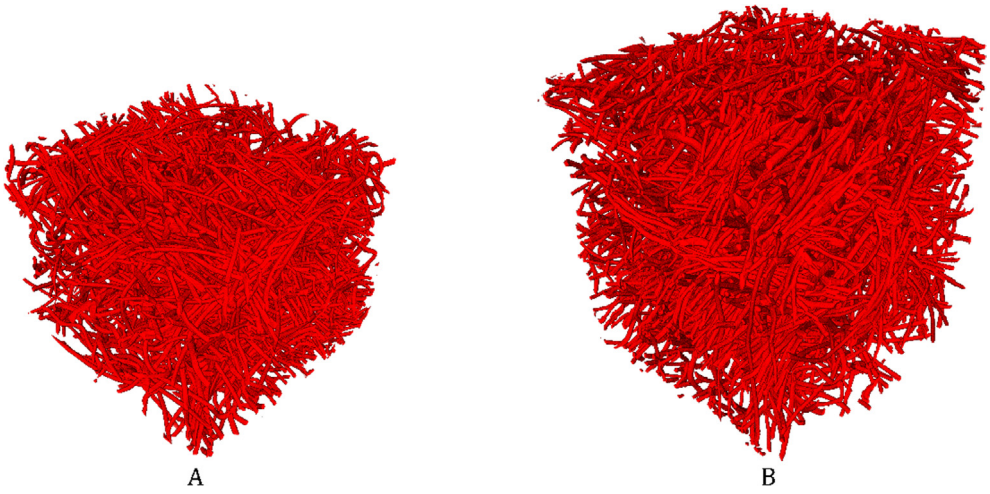

Fig. 4. 3D reconstruction of neat nonwoven samples A and B.

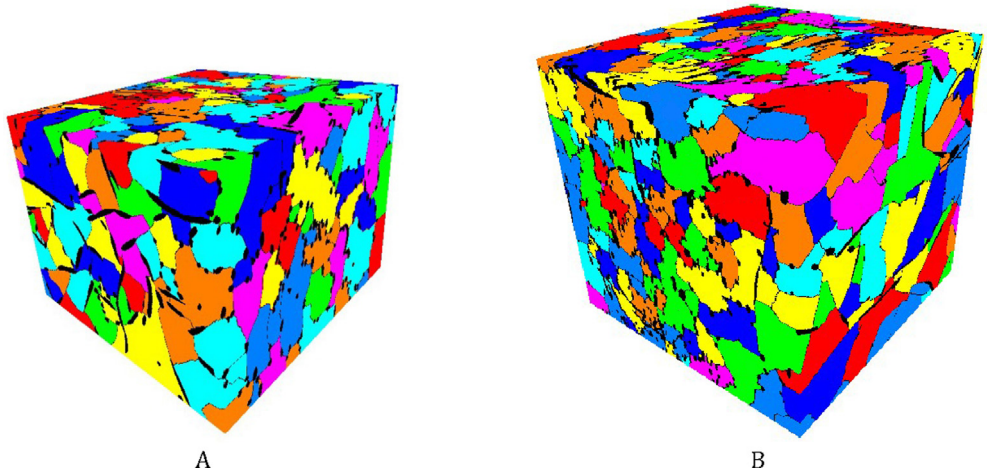

Fig. 5. Separated pores of samples A and B.

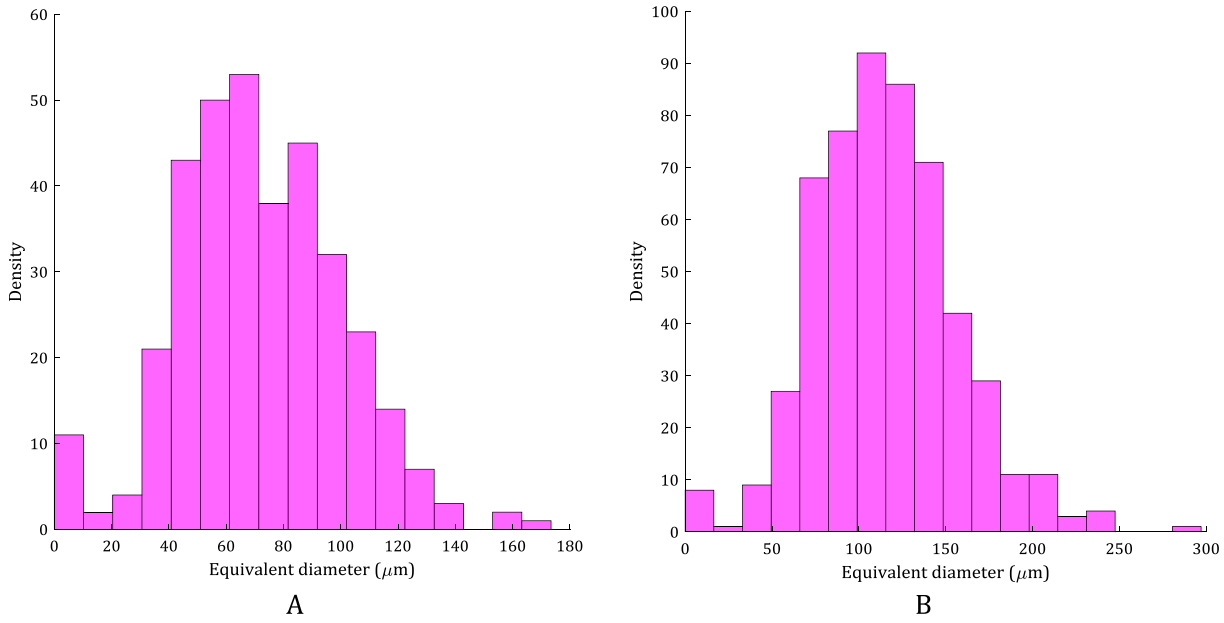

Fig. 6. Pore size distribution of samples A and B.

separated pores in close proximity are more likely to be shown in different colors. In this figure, black voxels represent fiber phase. Fig. 6 shows pore size distribution of nonwoven samples A and B calculated using Eq. (2).

As is observed, for both the samples, pore size distribution shows a Gaussian distribution. Mean pore size for samples A and B are 71.5 and 111.2 μm, respectively. Larger pore size of sample B is attributed to the lower fineness of fibers. For a given weight per unit area, the numbers of fibers present in the sample decrease as coarser fibers are used. In other words, coarser fibers lead to presence of fewer fibers per unit weight of the material and hence formation of larger pores.

The SEM micrographs of the neat nonwoven fabrics and aerogel blanket samples are presented in Fig. 7. The images clearly demonstrate the efficient fiber coating with aerogel particles. Moreover, as is observed the pores of the nonwoven fabric is mostly filled with the silica aerogels. As previously mentioned, the μCT device used for this study has a resolution of 1–3 μm. Therefore, this technique cannot be used for characterization of aerogels in the internal structure of blankets.

In order to investigate the effect of aerogel sol volume used in the immersion step of blankets, silica aerogel blankets were prepared by in situ synthesis of silica aerogel on samples A and B at three sol volumes of 14, 24 and 34 ml. For both the A and B samples, increase in sol volume used in the immersion step grows the content of aerogel particles. The results indicate that increasing sol volume from 14 to 24 ml improves the surface fiber coating. However, as shown in Fig. 7 further increase in sol volume may result in formation of big aerogel clusters in micro pores of nonwoven fabrics.

In order to investigate the effect of aerogel structure, samples AM-24, AC-24, AH-24, AI-24, BM-24, BC-24, BH-24 and BI-24 were synthesized in different conditions. It was found that the morphology of aerogel blankets is considerably affected with varying synthesis conditions. The results show the uniform distribution of silica aerogel particles and excellent fiber coating in silica aerogels M. This can be attributed to the appropriate content of water and catalyst in synthesis process which in turn results in complete sol-gel reactions of TEOS. Insufficient content of water and catalyst in synthesis process of aerogels C, H and I leads to agglomeration of aerogel particles and non-uniform fiber coating, which in turn results in formation of large pores in the blankets structure.

4.2. Structural and physical properties of the silica aerogel particles

Fig. 8 shows the nitrogen adsorption–desorption isotherms of the aerogel particles synthesized in different conditions. According to the International Union of Pure and Applied Chemistry (IUPAC) classification adsorption isotherms, type IV isotherm with different hysteresis loop can be observed for aerogel samples. Type IV isotherm confirms the presence of mesopores in the structure of silica aerogel particles [47]. The initial increase of the gas absorption is attributed to the presence of micropores inside the networks. However, according to IUPAC classification, the hysteresis loop type H3 for samples M and C indicate the existence of slit-shaped pores in their structure. Also, type H4 for sample H and type H2 for sample I reveal the presence of narrow slit pores and bottleneck constrictions in the structure, respectively. The physical and structural properties of silica aerogel particles are summarized in the Table 3 and pore size distribution of aerogels is shown in Fig. 9.

The specific surface area in the range of 782–977 m^2/g, mean pore diameter in the range of 6–22 nm and porosities higher than 80% are successfully achieved for all the silica aerogel particles synthesized in different conditions. The results clearly demonstrate the profound effect of synthesis conditions on the structural and physical properties of the silica aerogel particles. The effect of water and catalyst content on the structure of silica aerogel is displayed by the results of aerogel C, I, M and H. In the presence of large amount of water and catalyst in synthesis of aerogel M, the sol-gel process of TEOS is significantly accelerated and the time of gel formation is shortened. Therefore, a nanoporous structure with high pore volume of 2.70 cm^3/g and mean pore diameter of 22 nm with a wide pore size distribution is formed. In synthesis of aerogels C, I and H, insufficient water and catalyst leads to the incomplete hydrolysis and condensation reactions of TEOS. This consequently results in more gel shrinkage during the drying process and hence, non-uniform and dense structures with smaller pore sizes are obtained as compared with aerogel M.

Since strengthening of silica aerogel network occurs in the aging step of synthesis process, the aging condition has an intensive effect on the pore structure of silica aerogel. Also, the surface modification step as the main step of the silica aerogel synthesis via ambient pressure drying strongly affects the structure and properties of the silica aerogel. The solution of 77.5% EtOH + 15%

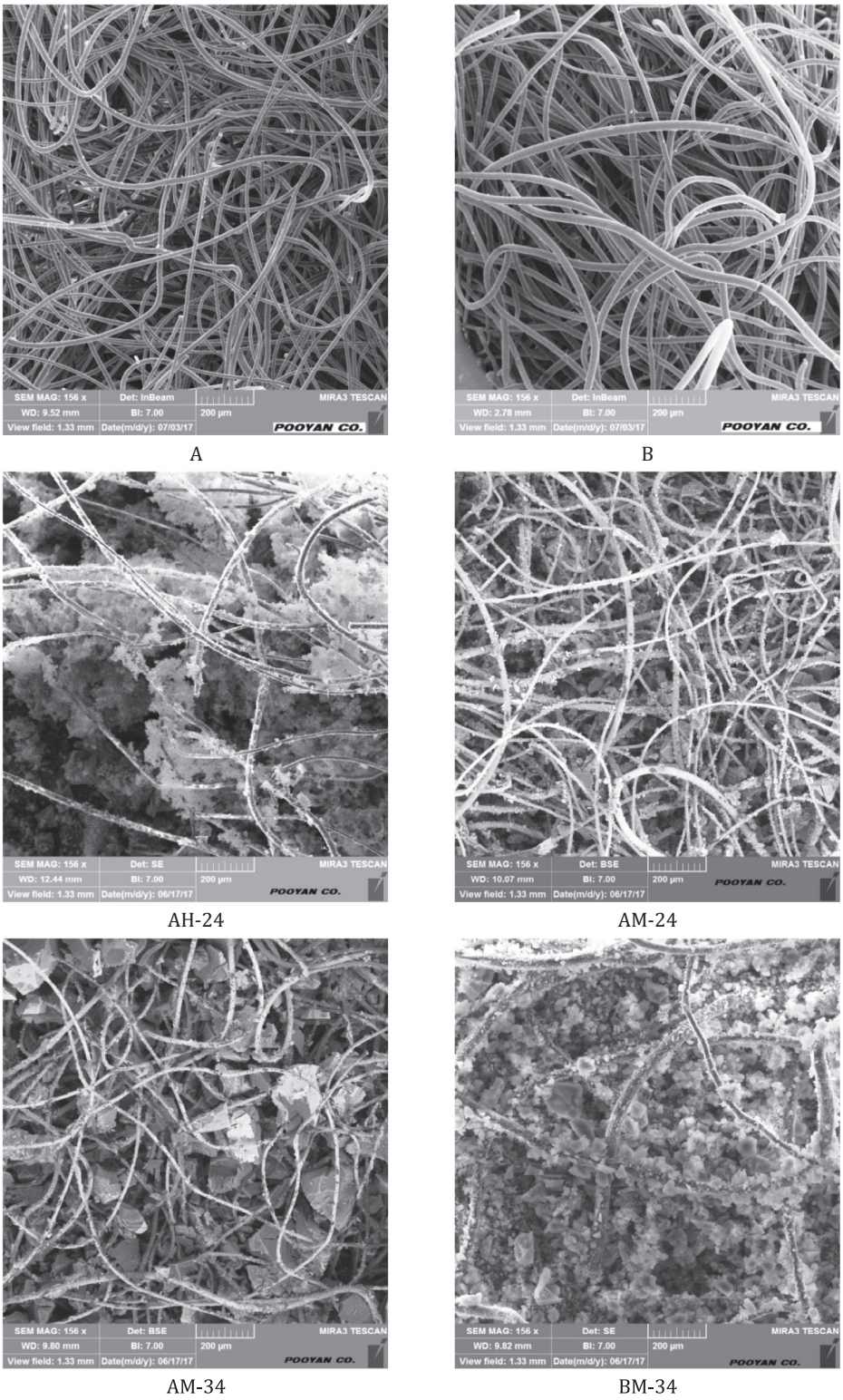

Fig. 7. SEM images of the neat nonwoven fabrics and aerogel blankets.

TEOS + 7.5% H_2O was used for ageing of aerogel I and its relevant blanket, while other samples were aged in ethanol. Additionally, the surface modification step was omitted from the synthesis process of sample I and its blankets. Generally, in the absence of surface modification, xerogel structure with micro pores and low porosity is expected to be formed. In this study mesoporous structure with porosity of 82%, pore size of 6 nm and pore volume of 1.64 cm^3/g is achieved for aerogel sample I. This can be attributed to the strengthening of silica gel network in the presence of TEOS in the aging solution which leads to less shrinkage in the drying step. On the other hand, using the surface modification step in the synthesis process has been caused the hydrophobic properties of aerogel samples C, M and H comparing to the hydrophilic aerogel I.

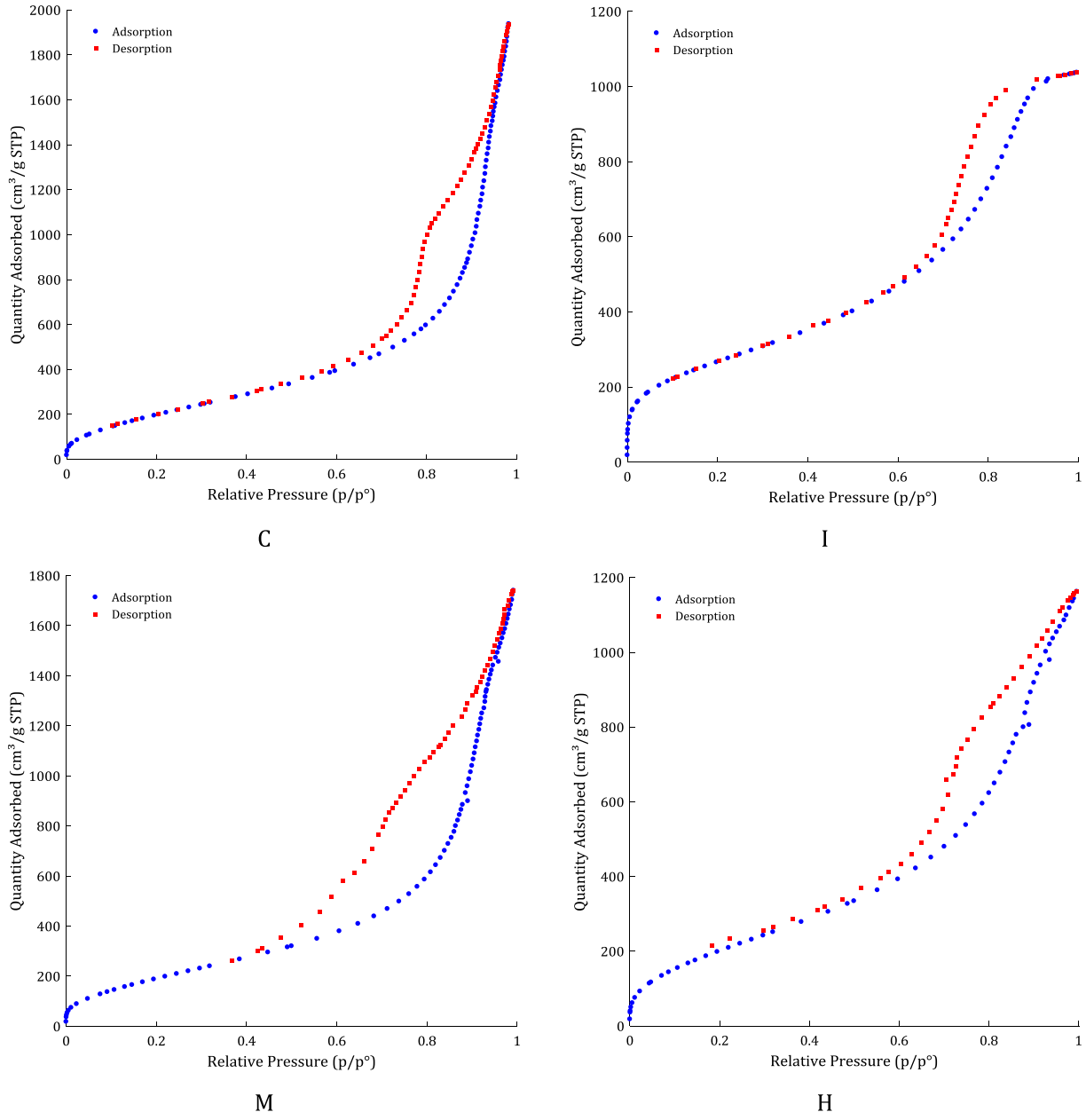

Fig. 8. Nitrogen adsorption–desorption isotherm of silica aerogel particles.

Table 3
Physical properties of the silica aerogels under different synthesis conditions.

Sample	Surface area (m^2/g)	pore volume (cm^3/g)	Mean pore diameter (nm)	Mean particle diameter (nm)	Bulk density (g/cm^3)	Porosity (%)
C	824	2.98	11	7	0.24 ± 0.021	89
I	977	1.64	6	6	0.39 ± 0.006	82
M	782	2.70	22	8	0.21 ± 0.008	90
H	811	1.82	8	7	0.33 ± 0.021	85

4.3. Hydrophobicity

The hydrophobic properties of samples evaluated using the water contact angle test. The images of water droplets on the blanket samples C, I and M are shown in Fig. 10. As can be observed, the aerogel blankets prepared by aerogels C and M clearly exhibit the high hydrophobicity with the contact angle of 145°, while sample I is completely hydrophilic and the added droplet is quickly absorbed by the sample. This can be attributed to the surface modification of silica wet gel with TMCS for aerogel blankets containing aerogel particles C, M and H. Successful surface modification of silica gel gives a rise the substitution of surface Si—OH groups with hydrophobic Si—O—CH3. Since surface modification by TMCS was not carried out for aerogel blanket containing aerogel particle I, this sample exhibits hydrophilic properties.

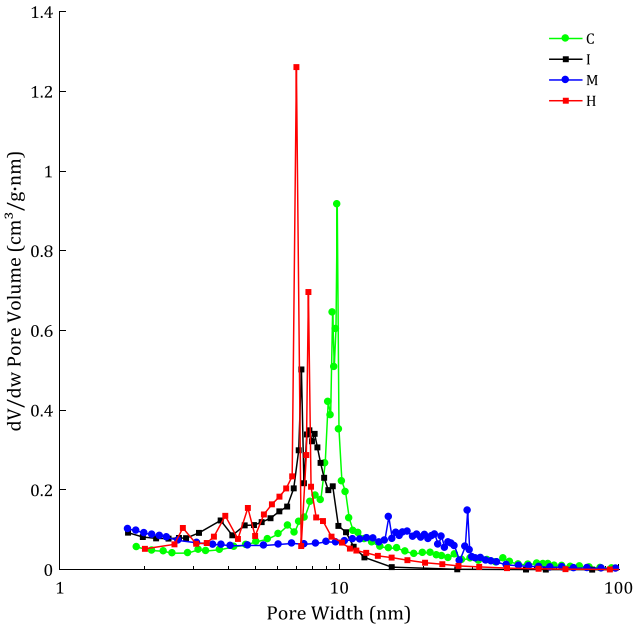

Fig. 9. Pore size distribution of silica aerogel particles at different synthesis conditions.

4.4. Sound absorption characteristics

Variation of SAC with frequency for samples A and B are presented in Fig. 11. As is observed at low frequencies both samples suffer from low SAC and SAC increases with increasing sound wave frequency. Generally, two different methods are used to reduce unwanted noise, namely passive and active noise control. Nonwoven fabric is a typical passive medium. Sound absorbability of passive media depends on the sound wave frequency. At high frequency levels, an adiabatic process occurs when the sound waves passes through the irregular structure of media. This causes reduction of sound energy by converting into heat. However, at low frequency levels the process is isothermal. Therefore, passive noise control is incapable of attenuating the low frequency noise unless very thick materials are used. Both samples A and B suffer from low absorption at low frequencies which is due to the small thickness of samples. As can be observed, sample B enjoys higher SAC as compared with sample A, which is mainly attributed to the higher thickness of sample B.

In this figure, SAC of both samples were also modeled using modified empirical model of Delaney and Bazley [48] which was suggested by Miki [49]. According to this model, for a layer of homogeneous porous media the characteristic impedance (Z_f), complex wave propagation constant $\left(\gamma_f\right)$, and surface acoustic impedance of the porous medium (Γ_f) can be expressed as Eqs. (3)–(5):

$$Z_f = \rho_a c_a \left[1 + 0.070\left(\frac{\rho_a f}{\sigma}\right)^{-0.632} - \mathrm{i}\,0.107\left(\frac{\rho_a f}{\sigma}\right)^{-0.632}\right] \tag{3}$$

$$\gamma_f = \frac{2\pi f}{c_a}\left[1 + 0.160\left(\frac{\rho_a f}{\sigma}\right)^{-0.618} - \mathrm{i}\,0.109\left(\frac{\rho_a f}{\sigma}\right)^{-0.618}\right] \tag{4}$$

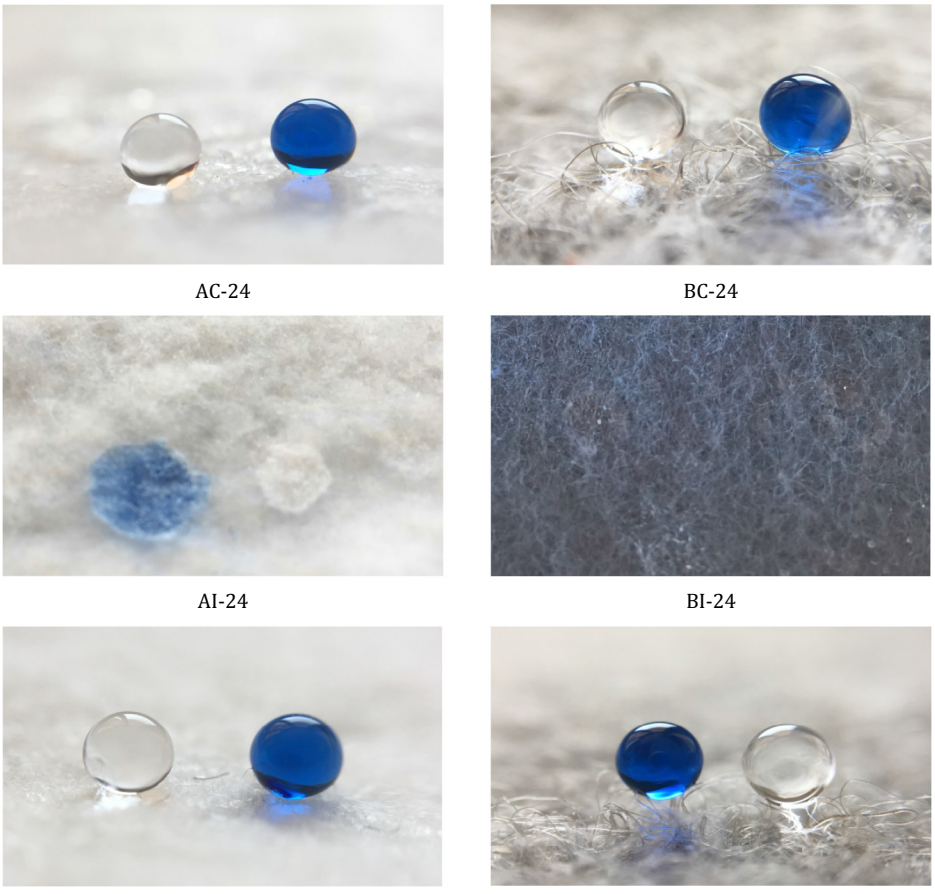

Fig. 10. Water droplets on the surface of the aerogel blankets.

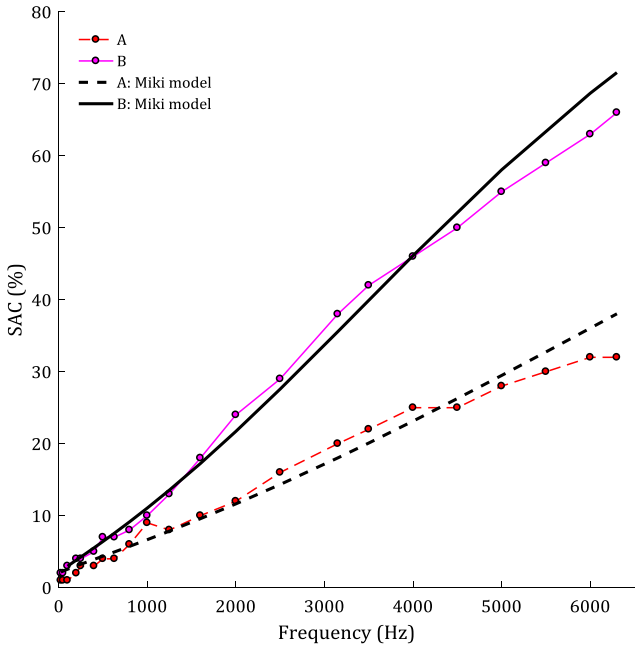

Fig. 11. Variation of SAC with frequency for neat nonwoven fabrics A and B.

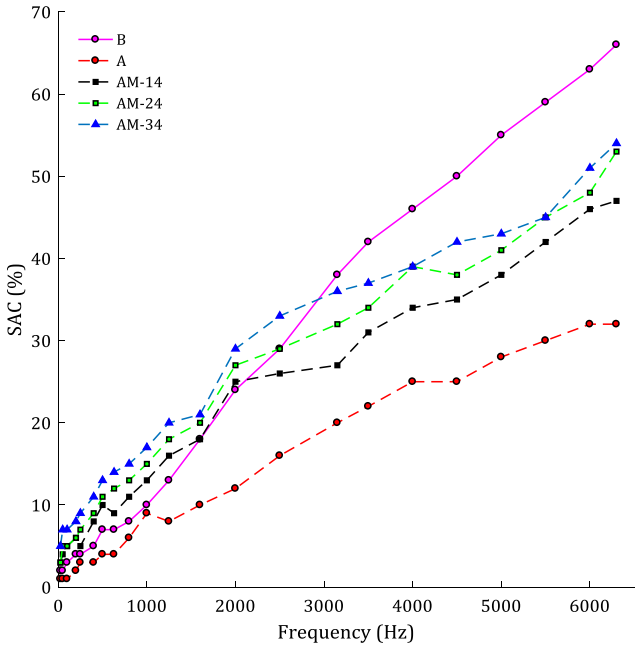

Fig. 12. Variation of SAC with frequency for neat nonwovens A and B and aerogel blankets synthesized with different sol volume.

$$\Gamma_f = i\, Z_f \tan\left(\frac{\pi}{2} + \gamma_f t_f\right) \tag{5}$$

where ρ_a denotes air density (kg/m^3), c_a is the velocity of sound in the air (m/s), f is sound wave frequency (Hz), σ represents flow resistivity (kg/m^3 s), and t_f is the thickness of porous media (m).

The sound absorption coefficient (SAC) is calculated using Eq. (6):

$$\mathrm{SAC} = \frac{4R_f/\rho_a c_a}{\left(1 + R_f/\rho_a c_a\right)^2 + \left(X_f/\rho_a c_a\right)^2} \tag{6}$$

where R_f and X_f are the real and imaginary components of surface acoustic impedance (Γ_f).

As can be observed sound absorption behavior of both samples can be modeled reasonably well using Miki model.

Variation of SAC with frequency for neat nonwovens A and B and aerogel blankets synthesized with different sol volume is shown in Fig. 12. As can be observed at all frequency levels aerogel blankets exhibit higher SAC than the neat nonwoven sample A. This is attributed to the low bulk density of silica aerogel. The low bulk density results in slow propagation of sound wave through the material and thus higher SAC. Moreover, coating of the fibers with silica aerogel effectively increases fiber diameter which in turn leads to reduction in pore size. Moreover, aerogel particles act as filling material among the fibers. This results in increasing tortuosity for the gas flow through the pore structure of aerogels. Thus, SAC enhances due to the induced viscous stresses as the result of friction between the air molecules and silica aerogels. On the other hand when the sound waves impinge the silica aerogel blankets, they get reflected within the blanket structure. The reflected sound energy is dissipated due to multiple internal reflections at the solid surfaces of structure that results in conversion of fluid kinetic energy into heat energy.

As is observed in Fig. 12, increase in sol volume leads to increase in SAC. With increasing the sol volume fiber diameter increases and pores in aerogel blankets become smaller and therefore due to the mentioned reasons SAC increases.

The importance of sample thickness in sound absorption lies in the fact that if a sound wave of wavelength l is to be damped, then the thickness of the sound absorbing material must be at least $l/2$. In other words, thicker materials are needed for low frequency sound adsorption since the wavelength increases by decreasing sound frequency [33]. As is observed, at low frequencies aerogel blankets A with lower thickness have better sound absorption ability than the neat nonwoven sample B. Thus coating of the nonwovens makes them particularly adapted to low-frequency sound control where space is a concern.

Variation of SAC with frequency for neat nonwoven B and its aerogel blankets synthesized with different sol volume is shown in Fig. 13. The results indicate that with increasing sol volume from

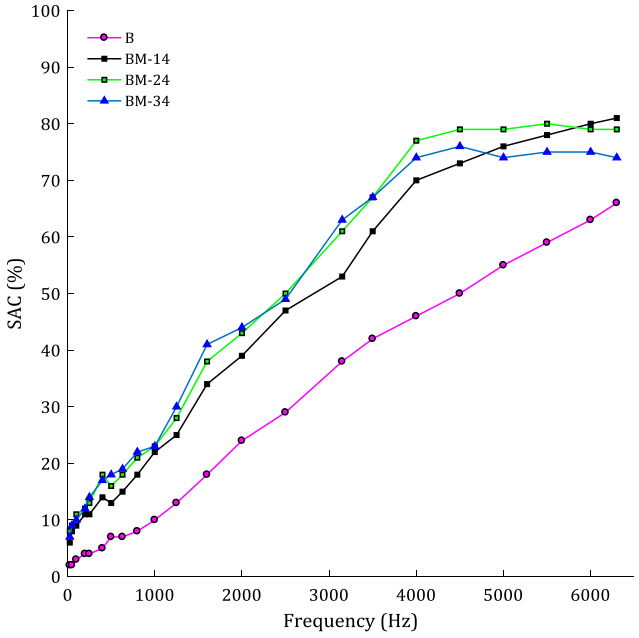

Fig. 13. Variation of SAC with frequency for neat nonwoven B and its aerogel blankets synthesized with different sol volume.

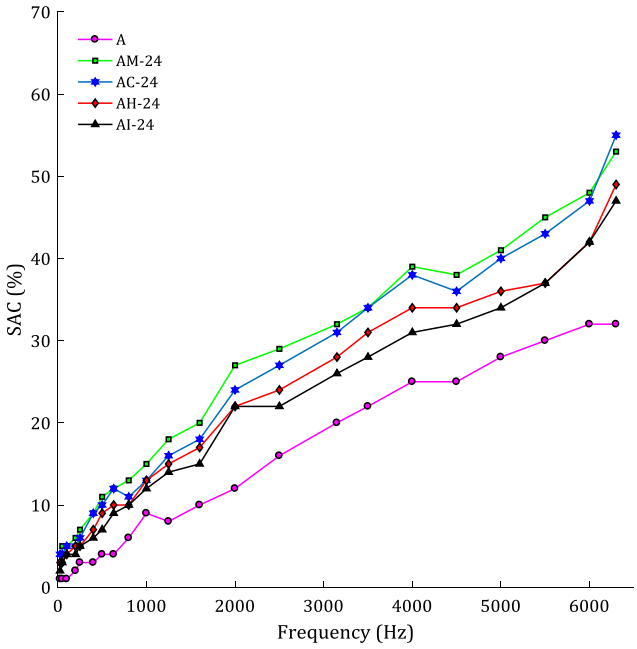

Fig. 14. Effect of aerogel structure on SAC of neat nonwoven A and aerogel blankets A.

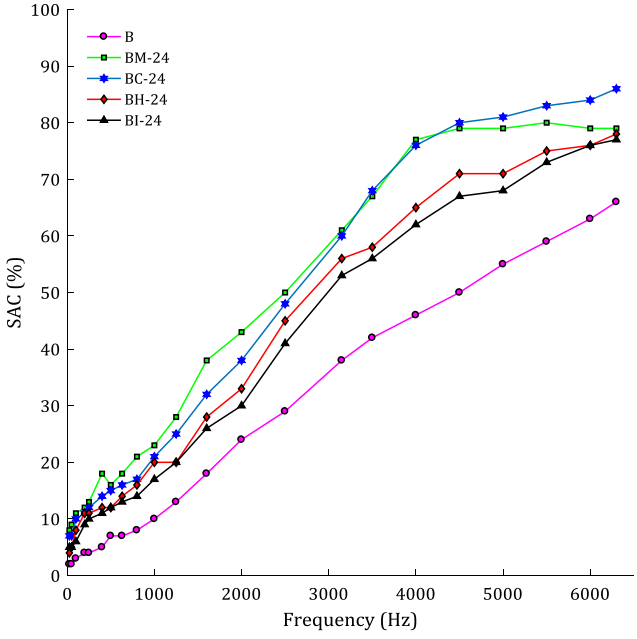

Fig. 15. Effect of aerogel structure on SAC of neat nonwoven B and aerogel blankets B.

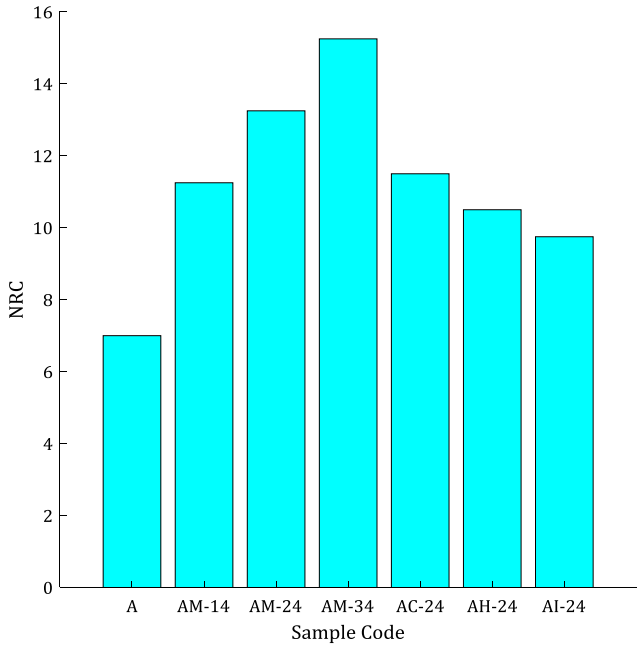

Fig. 16. NRC for neat nonwoven fabric A and aerogel blankets A.

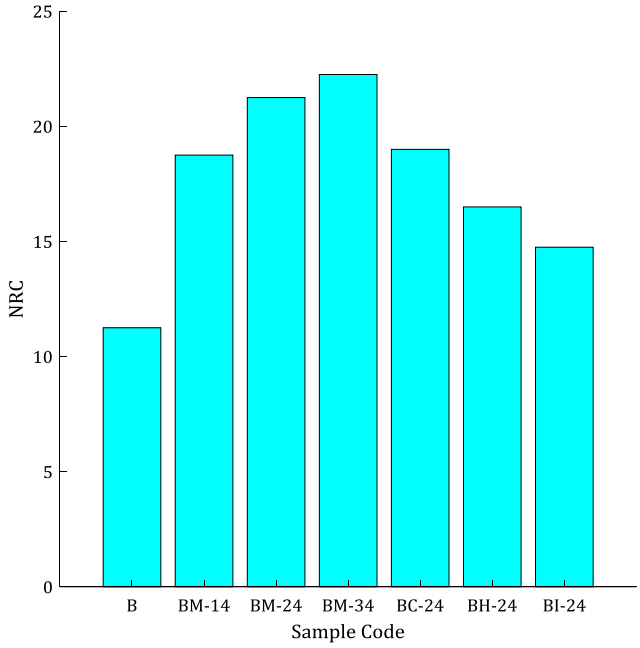

Fig. 17. NRC for neat nonwoven fabric B and aerogel blankets B.

14 to 24 ml, SAC enhances. However, further increase in sol volume from 24 to 34 ml not only necessarily improves SAC at low and mid frequencies, but also adversely affects SAC at high frequencies. This may be attributed to the larger diameter of fibers in sample B as compared with fibers diameter in sample A. Therefore, increasing sol volume to 34 ml results in formation of very small pores, as a result of which acoustic wave cannot efficiently penetrate into the blanket and reflects from the surface of the sample, hence decreasing SAC.

Effect of aerogel structure on SAC of aerogel blankets A and B is illustrated in Figs. 14 and 15. As is observed aerogel M exhibits the highest SAC, followed by aerogels C, H and I. This is attributed to the bulk density of aerogels. Aerogel M enjoys lowest bulk density, followed by aerogels C, H and I. Low bulk density causes sound travels very slowly through the materials which results in a higher SAC. Also higher porosity and larger pore size allow the sound wave to penetrate the structure much easier and therefore sound reflection from the surface of blankets decreases. The penetrated sound wave impinges the irregular internal structure of aerogel blanket. The sound pressure causes the air entrapped within the voids of the aerogel to vibrate. Sound energy is dissipated by the frictional resistance among the aerogels, fibers and the vibrating air and hence SAC increases.

Referring to Figs. 14 and 15, hydrophobic aerogel samples C, M and H enjoy higher SAC as compared with hydrophilic aerogels I.

Hydrophobic aerogels are protected against humidity and their structural integrity is sustained over long period of time, which in turn results in providing a long service life for sound absorption end-uses such as buildings.

In order to present a single number index of the sound-absorbing efficiency of nonwoven fabrics, SAC was measured at frequencies of 250, 500, 1000 and 2000 Hz and the results were averaged to obtain the noise reduction coefficient (NRC). Basically, NRC is a measurement of how well a media absorbs sound wave, mostly in the range of human speech frequencies. The results are presented in Figs. 16 and 17. As is observed, samples AM-34 and BM-34 enjoy the highest NRC.

5. Conclusion

This study investigated the sound absorption behavior of silica aerogel/PET blankets. An industrial scale melt spinning line was used to produce PET fibers. Afterwards, nonwoven fabrics were produces using a laboratory scale needling line. Realistic 3D images of nonwoven fabrics were obtained using μCT technique and fabrics were characterized in terms of thickness, porosity, pore size and fiber diameter.

The silica aerogel blankets were prepared by *in situ* synthesis of silica aerogel on the nonwoven fabrics via a two-step sol-gel process of TEOS which was followed by drying at ambient pressure. Specific surface area and pore structure of aerogels were determined using nitrogen adsorption analysis. It was established that synthesis conditions has a strong effect on the morphology of aerogels. Uniform distribution of silica aerogel particles and fiber coating was observed for the blanket sample synthesized with higher water and catalyst content. Improvement in the surface fiber coating was observed with increasing the sol volume from 14 to 24 ml.

SACs of the aerogel blankets over the entire frequency range of 50–6100 Hz were measured using a double-microphones standing wave impedance tube. Effect of sol volume and synthesis condition on the acoustical properties of aerogel blankets was investigated. The results indicated that at all frequency levels aerogel blankets exhibit higher SAC than the neat nonwoven samples. This was attributed to the low bulk density of silica aerogel, reduction in pore size and increase in tortuosity of blankets. The results indicated that aerogel particles M with the lowest bulk density enjoy the highest SAC. It was found that for aerogel blankets A, at all frequency levels increase in sol volume leads to increase in SAC. However, for aerogel blankets B, increase in sol volume increases SAC up to 24 ml, beyond which SAC reduces at high frequencies. It was also found that aerogel coating of the nonwoven fabrics makes them particularly adapted to low-frequency sound control where space is a concern. Considering the results, for the investigated samples, aerogel M with sol volume of 24 ml is recommended for synthesis on nonwoven samples. This is due to the fact that this aerogel not only leads to higher SAC, but also due to its hydrophobic characteristics provides a long service life for sound absorption end-uses.

Declaration of Competing Interest

None.

Acknowledgements

The authors greatly appreciate the guidance and help given by Professor Mohammad Zarrebini during the course of research.

Funding

This research did not receive any specific grant from funding agencies in the public, commercial, or not-for-profit sectors.

Appendix A. Supplementary data

Supplementary data to this article can be found online at https://doi.org/10.1016/j.conbuildmat.2019.06.031.

References

[1] P. Soltani, M. Zerrebini, The analysis of acoustical characteristics and sound absorption coefficient of woven fabrics, Text. Res. J. 82 (2012) 875–882.
[2] F. Shahani, P. Soltani, M. Zarrebini, The analysis of acoustic characteristics and sound absorption coefficient of needle punched nonwoven fabrics, J. Eng. Fibers Fabr. 9 (2014) 84–92.
[3] X. Liu, X. Yan, H. Zhang, Effects of pore structure on sound absorption of kapok-based fiber nonwoven fabrics at low frequency, Text. Res. J. 86 (2016) 755–764.
[4] T. Yang, X. Xiong, R. Mishra, J. Novák, J. Militký, Acoustic evaluation of Struto nonwovens and their relationship with thermal properties, Text. Res. J. (2016) 426–437.
[5] S. Rwawiire, B. Tomkova, J. Militky, L. Hes, B.M. Kale, Acoustic and thermal properties of a cellulose nonwoven natural fabric, Appl. Acoust. 116 (2017) 177–183.
[6] O. Kinnane, A. Reilly, J. Grimes, S. Pavia, R. Walker, Acoustic absorption of hemp-lime construction, Constr. Build. Mater. 122 (2016) 674–682.
[7] D.A. Bies, C. Hansen, C. Howard, Engineering Noise Control, CRC Press, New York, 2017.
[8] L. Wang, F.-S. Zhang, Characterization of a novel sound absorption material derived from waste agricultural film, Constr. Build. Mater. 157 (2017) 237–243.
[9] A.D. Pierce, R.T. Beyer, Acoustics: An Introduction to its Physical Principles and Applications, ASA, New York, 1990.
[10] S. Malakooti, H.G. Churu, A. Lee, T. Xu, H. Luo, N. Xiang, C. Sotiriou-Leventis, N. Leventis, H. Lu, Sound insulation properties in low-density, mechanically strong and ductile nanoporous polyurea aerogels, J. Non-Cryst. Solids 476 (2017) 36–45.
[11] J.-O. Yeon, K.-W. Kim, K.-S. Yang, J.-M. Kim, M.-J. Kim, Physical properties of cellulose sound absorbers produced using recycled paper, Constr. Build. Mater. 70 (2014) 494–500.
[12] C. Zhao, Y. Yan, Z. Hu, L. Li, X. Fan, Preparation and characterization of granular silica aerogel/polyisocyanurate rigid foam composites, Constr. Build. Mater. 93 (2015) 309–316.
[13] M.G. Gomes, I. Flores-Colen, F. da Silva, M. Pedroso, Thermal conductivity measurement of thermal insulating mortars with EPS and silica aerogel by steady-state and transient methods, Constr. Build. Mater. 172 (2018) 696–705.
[14] E. Moretti, F. Merli, E. Cuce, C. Buratti, Thermal and acoustic properties of aerogels: preliminary investigation of the influence of granule size, Energy Procedia 111 (2017) 472–480.
[15] E. Lucchi, F. Becherini, M.C. Di Tuccio, A. Troi, J. Frick, F. Roberti, C. Hermann, I. Fairnington, G. Mezzasalma, L. Pockelé, A. Bernardi, Thermal performance evaluation and comfort assessment of advanced aerogel as blown-in insulation for historic buildings, Build. Environ. 122 (2017) 258–268.
[16] Y. Liang, H. Wu, G. Huang, J. Yang, H. Wang, Thermal performance and service life of vacuum insulation panels with aerogel composite cores, Energy Build. 154 (2017) 606–617.
[17] T.-G. Kim, C.-W. Park, J.-G. Lee, M.-W. Kim, M.S. Choi, W.Y. Kim, J.S. Yang, S.S. Yoon, Supersonically sprayed clay, silica, and silica aerogel hybrid films as thermal and electrical barriers, Ceram. Int. 44 (2018) 12934–12939.
[18] N. Abbas, H.R. Khalid, G. Ban, H.T. Kim, H. Lee, Silica aerogel derived from rice husk: an aggregate replacer for lightweight and thermally insulating cement-based composites, Constr. Build. Mater. 195 (2019) 312–322.
[19] Z.-H. Liu, Y.-D. Ding, F. Wang, Z.-P. Deng, Thermal insulation material based on SiO2 aerogel, Constr. Build. Mater. 122 (2016) 548–555.
[20] M. Sachithanadam, S.C. Joshi, Effect of granule sizes on acoustic properties of protein-based silica aerogel composites via novel inferential transmission loss method, Gels 2 (2016) 11.
[21] C. Buratti, F. Merli, E. Moretti, Aerogel-based materials for building applications: influence of granule size on thermal and acoustic performance, Energy Build. 152 (2017) 472–482.
[22] N. Bheekhun, A. Talib, A. Rahim, M.R. Hassan, Aerogels in aerospace: an overview, Adv. Mater. Sci. Eng. 2013 (2013) 1–18.
[23] F. Cotana, A.L. Pisello, E. Moretti, C. Buratti, Multipurpose characterization of glazing systems with silica aerogel: in-field experimental analysis of thermal-energy, lighting and acoustic performance, Build. Environ. 81 (2014) 92–102.
[24] M. Ramamoorthy, A.A. Pisal, R.S. Rengasamy, A.V. Rao, In-situ synthesis of silica aerogel in polyethylene terephthalate fibre nonwovens and their composite properties on acoustical absorption behavior, J. Porous Mater. 25 (2018) 179–187.
[25] J. Gross, J. Fricke, L.W. Hrubesh, Sound propagation in SiO2 aerogels, J. Acoust. Soc. Am. 91 (1992) 2004–2006.
[26] L. Forest, V. Gibiat, T. Woignier, Evolution of the acoustical properties of silica alcogels during their formation, Ultrasonics 36 (1998) 477–481.
[27] E.T. Afriyie, P. Karami, P. Norberg, K. Gudmundsson, Textural and thermal conductivity properties of a low density mesoporous silica material, Energy Build. 75 (2014) 210–215.

[28] L. Forest, V. Gibiat, A. Hooley, Impedance matching and acoustic absorption in granular layers of silica aerogels, J. Non-Cryst. Solids 285 (2001) 230–235.
[29] S.B. Riffat, G. Qiu, A review of state-of-the-art aerogel applications in buildings, Int. J. Low-Carbon Technol. 8 (2012) 1–6.
[30] M.A. Aegerter, N. Leventis, M.M. Koebel, Aerogels Handbook, Springer Science & Business Media, New York, 2011.
[31] Z.M.-s. Talebi, A.M. Shoushtari, A.R. Bahramian, M. Abdouss, Synthesis, pore structure and properties of polyurethane/silica hybrid aerogels dried at ambient pressure, J. Ind. Eng. Chem. 21 (2015) 797–804.
[32] A. Tadjarodi, M. Haghverdi, V. Mohammadi, Preparation and characterization of nano-porous silica aerogel from rice husk ash by drying at atmospheric pressure, Mater. Res. Bull. 47 (2012) 2584–2589.
[33] S. Motahari, H. Javadi, A. Motahari, Silica-aerogel cotton composites as sound absorber, J. Mater. Civ. Eng. 27 (2014) 1–6.
[34] N. Eskandari, S. Motahari, Z. Atoufi, G. Hashemi Motlagh, M. Najafi, Thermal, mechanical, and acoustic properties of silica aerogel/UPVC composites, J. Appl. Polym. Sci. 134 (2017) 1–8.
[35] T. Yang, X. Xiong, M. Venkataraman, R. Mishra, J. Novák, J. Militký, Investigation on sound absorption properties of aerogel/polymer nonwovens, J. Text. Inst. (2018) 1–6.
[36] C. Buratti, E. Moretti, Experimental performance evaluation of aerogel glazing systems, Appl. Energy 97 (2012) 430–437.
[37] C. Buratti, E. Moretti, Glazing systems with silica aerogel for energy savings in buildings, Appl. Energy 98 (2012) 396–403.
[38] A.V. Rao, M.M. Kulkarni, G.M. Pajonk, D.P. Amalnerkar, T. Seth, Synthesis and characterization of hydrophobic silica aerogels using trimethylethoxysilane as a co-precursor, J. Sol-Gel Sci. Technol. 27 (2003) 103–109.
[39] P. Soltani, M. Zarrebini, R. Laghaei, A. Hassanpour, Prediction of permeability of realistic and virtual layered nonwovens using combined application of X-ray μCT and computer simulation, Chem. Eng. Res. Des. 124 (2017) 299–312.
[40] Z.M.-s. Talebi, A.M. Shoushtari, M. Abdouss, A.R. Bahramian, Relationship analysis of processing parameters with micro and macro structure of silica aerogel dried at ambient pressure, J. Non-Cryst. Solids 376 (2013) 30–37.
[41] F. Latifi, Z.M.-s. Talebi, H. Khalili, M. Zarrebini, Effect of processing parameters and pore structure of nanostructured silica aerogel on the physical properties of aerogel blankets, Mater. Res. Express 5 (2018) 1–11.
[42] R. Pashminehazar, A. Kharaghani, E. Tsotsas, Three dimensional characterization of morphology and internal structure of soft material agglomerates produced in spray fluidized bed by X-ray tomography, Powder Technol. 300 (2016) 46–60.
[43] P. Soltani, M.S. Johari, M. Zarrebini, Tomography-based determination of transverse permeability in fibrous porous media, J. Ind. Text. 44 (2015) 738–756.
[44] P. Soltani, M.S. Johari, M. Zarrebini, Effect of 3D fiber orientation on permeability of realistic fibrous porous networks, Powder Technol. 254 (2014) 44–56.
[45] P. Soltani, M. Azimian, A. Wiegmann, M. Zarrebini, Experimental and computational analysis of sound absorption behavior in needled nonwovens, J. Sound Vib. 426 (2018) 1–18.
[46] A.P. Mangan, R.T. Whitaker, Partitioning 3D surface meshes using watershed segmentation, IEEE Trans. Visual Comput. Graphics 5 (1999) 308–321.
[47] Z.M.-s. Talebi, A.M. Shoushtari, A.R. Bahramian, M. Abdouss, Synthesis, structure and thermal protective behavior of silica aerogel/PET nonwoven fiber composite, Fibers Polym. 15 (2014) 2154–2159.
[48] M.E. Delany, E.N. Bazley, Acoustical properties of fibrous absorbent materials, Appl. Acoust. 3 (1970) 105–116.
[49] Y. Miki, Acoustical properties of porous materials: modifications of Delany-Bazley models, J. Acoust. Soc. Jpn. (E) 11 (1990) 19–24.